*Shock Dynamics Center Internal Report 96-XX*

# Material Models for Sapphire, $\alpha$-Quartz, Lithium Fluoride, and Fused Silica for Use in Shock Wave Experiments and Wave Code Calculations

**R. Feng and Y. M. Gupta**

December, 1996

## A. Introduction:

This internal report describes material models for sapphire, $\alpha$-quartz and lithium fluoride (LiF) single crystals, and fused silica for the use in designing shock wave experiments and wave code computations. Here we consider primarily the one-dimensional (1-D) COPS code calculations. The models for the first two materials are limited for elastic response. Both the results derived from shock wave measurements[1-3] and from calculations using elastic constants to third or fourth order[4-9] are presented. For sapphire, approximation models useful for two-dimensional (2-D) calculations are also given. The model for LiF is only useful for shock compression along $\langle 100 \rangle$ orientation. The material is treated as a fluid[10,11] because the Hugoniot elastic limit (HEL) of a pure LiF crystal in $\langle 100 \rangle$ direction is negligibly small. Fused silica is modeled as a non-linear elastic material using both the shock compression data[1] and compression-shear wave measurements.[12]

## B. Finite-Strain Calculation for Anisotropic Elastic Response

Using a Taylor series expansion, we can write the Cauchy stress, $\sigma_{ij}$ in an elastic solid subjected to an adiabatic dynamic deformation as functions of the Green strain, $\eta_{ij}$ and the isentropic elastic constants, *i.e.*,[5]

$$\sigma_{ij} = \frac{1}{J} F_{ik} F_{jl} \left( C^S_{klmn} \eta_{mn} + \frac{1}{2} C^S_{klmnpq} \eta_{mn} \eta_{pq} + \frac{1}{6} C^S_{klmnpqrs} \eta_{mn} \eta_{pq} \eta_{rs} + \cdots \right), \tag{1}$$

where $F_{ij} = \partial x_i / \partial a_j$ is the deformation gradient tensor with $x_i$ and $a_i$ being the position vectors in the deformed and initial configurations, respectively, $J$ $(= \det \mathbf{F})$ is the Jacobian, and $C^S_{ijkl}$, $C^S_{ijklmn}$ and $C^S_{ijklmnpq}$ are the fourth, sixth and eighth rank isentropic elasticity tensors, respectively. The summation convention has been used. The definition of the Green strain is

$$\eta_{ij} = \frac{1}{2} \left( \frac{\partial x_k}{\partial a_i} \frac{\partial x_k}{\partial a_j} - \delta_{ij} \right), \tag{2}$$

where $\delta_{ij}$ is the identity tensor. Further details can be seen in Ref. 5.

Both sapphire and $\alpha$-quartz are trigonal crystals. Hence, two crystallography directions can be set coincide with the Cartesian coordinate so that $x_1$ is a specific direction in the basal plane of the hexagonal structure ($x$) and $x_3$ is that going out the plane ($z$). Along the $x_3$ axis and any directions in the basal plane, wave propagation modes are separated. Along any other directions, wave modes are coupled. For the purpose of this report, we consider primarily the material response under uniaxial compression along the $x_1$ or $x_3$ axis. Because a trigonal crystal is transversely isotropic about the $x_3$ ($z$) axis. The following symmetry applies:

$$C^S_{1133} = C^S_{2233} = C^S_{3311}, \tag{3a}$$

$$C^S_{111122} = C^S_{221111}, \tag{3b}$$

$$C^S_{111133} = C^S_{331111}, \tag{3c}$$

$$C^S_{113333} = C^S_{223333}, \tag{3d}$$

and so forth.

**1) Uniaxial compression along $x_3$ ($z$) axis:**

For this particular situation, only non-zero components of the deformation gradient are $F_{11} = F_{22} = 1$ and $F_{33} = V/V_0$, where $V$ and $V_0$ are the current and initial specific volumes, respectively. Hence, $J = V/V_0$ and the only non-zero component of the Green strain is $\eta_{33}$. Consequently, non-zero stress components (up to third-order strain) are:

$$\sigma_{11} = \frac{V_0}{V}\left(C^S_{1133}\eta_{33} + \frac{1}{2}C^S_{113333}\eta^2_{33} + \frac{1}{6}C_{11333333}\eta^3_{33}\right), \tag{4a}$$

$$\sigma_{22} = \frac{V_0}{V}\left(C^S_{2233}\eta_{33} + \frac{1}{2}C^S_{223333}\eta^2_{33} + \frac{1}{6}C^S_{22333333}\eta^3_{33}\right), \tag{4b}$$

$$\sigma_{33} = \frac{V}{V_0}\left(C^S_{3333}\eta_{33} + \frac{1}{2}C^S_{333333}\eta^2_{33} + \frac{1}{6}C^S_{33333333}\eta^3_{33}\right), \tag{4c}$$

with

$$\eta_{33} = -\frac{(2+\mu)\mu}{2(1+\mu)^2}, \tag{4d}$$

where $\mu\ (= V_0/V - 1)$ is the volume compression.

**2) Uniaxial compression along $x_1$ ($x$) axis:**

Non-zero components of the deformation and strain are $F_{11} = V/V_0$, $F_{22} = F_{33} = 1$ and $\eta_{11}$, respectively. The Jacobian is $J = V/V_0$. Hence, non-zero stress components (up to third-order strain) are:

$$\sigma_{11} = \frac{V}{V_0}\left(C^S_{1111}\eta_{11} + \frac{1}{2}C^S_{111111}\eta_{11}^2 + \frac{1}{6}C_{11111111}\eta_{11}^3\right), \tag{5a}$$

$$\sigma_{22} = \frac{V_0}{V}\left(C^S_{2211}\eta_{11} + \frac{1}{2}C^S_{221111}\eta_{11}^2 + \frac{1}{6}C^S_{22111111}\eta_{11}^3\right), \tag{5b}$$

$$\sigma_{33} = \frac{V_0}{V}\left(C^S_{3311}\eta_{11} + \frac{1}{2}C^S_{331111}\eta_{11}^2 + \frac{1}{6}C^S_{33111111}\eta_{11}^3\right), \tag{5c}$$

with

$$\eta_{11} = -\frac{(2+\mu)\mu}{2(1+\mu)^2}. \tag{5d}$$

## C. Models for Sapphire

**1) Hugoniot equations for designing experiment:**

The shock response of $z$-cut sapphire was characterized in Ref. 1. The reported HEL value for the material is in the range of 120 to 150 kbar. The elastic shock response of the material can be expressed as

$$U_S^e = c_L + u_p, \tag{6}$$

where $U_S^e$ is the elastic shock wave speed, $c_L$ (= 11.19 mm/μs) is the initial longitudinal sound speed, and $u_p$ is the particle velocity. The initial density of the material is $\rho_0 = 3.985$ g/cm$^3$. Hence, the shock stress (compressive longitudinal stress), $\sigma_c$ based on the jump conditions is simply

$$\sigma_c = \rho_0 U_S^e u_p = 445.9u_p + 39.85u_p^2 \text{ (kbar)}, \tag{7}$$

or

$$\sigma_c = \rho_0 c_L^2 (1+\mu)\mu = 4990(1+\mu)\mu \text{ (kbar)}. \tag{8}$$

The result of (8) is plotted in Fig. 1 as the dotted line. As demonstrated in the following, for a very good approximation, Equations (6) to (8) can also be used in designing experiments involving shock compression of sapphire along the $x$ axis.

**2) Models for 1-D wave code computation:**

A finite-strain treatment as presented in Section B is used for this purpose. Because the elastic response of the material is not significantly non-linear. A calculation up to second-order strain as done in Ref. 4 is sufficiently accurate. The initial longitudinal sound speed along the $z$ axis yields $C^S_{3333} = 4990$ kbar. The reset of the necessary constants are given in Ref. 6:

$$C^S_{1111} = 4968 \text{ kbar},\ C^S_{1122} = 1636 \text{ kbar},\ C^S_{1133} = 1109 \text{ kbar},$$

$$C^S_{111122} = -10900 \text{ kbar},\ C^S_{111133} = -9630 \text{ kbar},\ C^S_{113333} = -9220 \text{ kbar},$$

$$C^S_{111111} = -38700 \text{ kbar, and } C^S_{333333} = -33400 \text{ kbar}.$$

The resultant compressive longitudinal stress for uniaxial compression along the $z$ or $x$ axis ($-\sigma_{33}$ or $-\sigma_{11}$, respectively) and the corresponding mean stress ($-\sigma_{mm}/3$) are also presented in Fig. 1. The longitudinal response of $z$-axis compression is very close to that of $x$-axis compression, indicating that the longitudinal response of the material is essentially the same for uniaxial compression along any direction. However, the two mean stresses are noticeably different. In general, the mean stress response of an anisotropic crystal under uniaxial compression depends on the compression direction. Such a response is also expected to be different from the pressure response of the material under the hydrostatic or hydrodynamic compression.

To implement these results to the COPS code, we use *isotropic* models that effectively produce the same response under $x$-axis or $z$-axis compression. Two steps are involved: 1) Fit the mean stress-volume compression relation into a cubic function while fixing the first term coefficient according to the *second* order elastic constants. 2) Determine an *equivalent* shear modulus as a quadratic function of the mean stress from the difference between the longitudinal and mean stresses as if the material is an isotropic elastic solid. The results are as follows.

For *z-axis compression*, the Hugoniot mean stress is

$$P_H = 2403\mu + 4055\mu^2 - 17490\mu^3 \text{ (kbar)}. \qquad (9)$$

The equivalent shear modulus is

$$G = 1940 + 0.8443P - 7.688\times10^{-3}P^2 \text{ (kbar)}, \tag{10}$$

where $P$ is the thermodynamic mean stress calculated through the following Mie-Gruneisen equation of state:

$$(P - P_H) = \frac{\Gamma}{V}(E - E_H), \tag{11}$$

where subscript "$H$" denotes the quantities along the Hugoniot curve, $E$ is the internal energy per unit mass, and $\Gamma$ is the Gruneisen parameter. For sapphire, $\Gamma/V = 2.42$ g/cm$^3$ as reported in Ref. 13 and used in the SHOCKUP code. Note, that for sapphire within its elastic response, the thermodynamic influence is negligibly small.

For *x-axis compression*, the Hugoniot mean stress is

$$P_H = 2571\mu + 5246\mu^2 - 22020\mu^3 \text{ (kbar)}, \tag{12}$$

and the equivalent shear modulus is

$$G = 1798 + 1.562P - 7.942\times10^{-3}P^2 \text{ (kbar)}. \tag{13}$$

Here $P$ and $P_H$ are related again via (11). In Fig. 2, the peak state results calculated using (9) and (10), and (12) and (13) (the dashed lines) are compared with the calculations using elastic constants to third order (the solid lines). Within the stress range of interest, the two are practically identical.

Note, that the coefficients of the third order terms in (9) and (12) are negative. Hence, extension to higher stresses needs to be treated with caution. For $z$-axis compression, an earlier model,

$$P_H = 2403\mu + 3625\mu^2 \text{ (kbar)}$$

and

$$G = 1940 \text{ kbar}$$

though slightly less accurate is more robust at higher stresses than (9) and (10). However, when the calculated stress history is known to be within 150 kbar, (9) and (10) should be used for improved accuracy.

**3) Models for 2-D wave code computation:**

The pressure response of sapphire under hydrostatic compression was measured by d'Amour *et al.*[14] The reported initial bulk modulus, $K_0$ for the material is 2544 kbar. The value calculated using the second order elastic constants (see previous subsection) and the following equation,

$$K_0 = \frac{C^S_{3333}(C^S_{1111} + C^S_{1122}) - 2(C^S_{1133})^2}{C^S_{1111} + C^S_{1122} + 2C^S_{3333} - 4C^S_{1133}} \tag{14}$$

is 2510 kbar. The two are in very good agreement. If the hydrostatic data are fitted with the Birch-Murnaghan equation, *i.e.*,[14-16]

$$\sigma = \frac{3}{2}K_0\left[\left(\frac{V}{V_0}\right)^{-\frac{7}{3}} - \left(\frac{V}{V_0}\right)^{-\frac{5}{3}}\right]\left\{1 - \frac{3}{4}(4 - K_0')\left[\left(\frac{V}{V_0}\right)^{-\frac{2}{3}} - 1\right] + \cdots\right\}, \tag{15}$$

where $\sigma$ is the pressure, then the second order coefficient, $K_0'$ is 4.275.[14] The corresponding $\sigma - \mu$ relation is plotted in Fig. 3 in comparison with the uniaxial compression response along the $x$ or $z$ axis. Clearly, the hydrostatic response is very close to the mean stress response under uniaxial compression along the $x$-axis. The implication is that as long as the compression along the $z$-axis is not significantly larger than the other directions the hydrostatic response from Ref. 14 is a good approximation to the mean stress response of sapphire under multiaxial compression. Based on this observation, the following models are proposed for the use in 2-D calculations:

$$P_H = 2544\mu + 4166\mu^2 + 1350\mu^3 \text{ (kbar)}, \tag{16}$$

which is a direct fit to the hydrostatic response.[14] If the largest compression is along a direction in the crystal basal plane, then

$$G = 1818 + 2.246P - 1.613\times10^{-2}P^2 \text{ (kbar)}. \tag{17}$$

If the largest compression is along the $z$-axis, then

$$G = 1835 + 0.6505P - 1.254\times10^{-2}P^2 \text{ (kbar)}. \tag{18}$$

Here $P$ and $P_H$ are related again via (11). The results are also shown in Fig. 3 as the dashed lines. Note, that these models are approximations. Without rigorous 3-D calculation, it is difficult to quantitatively evaluate the models. If the conditions for using (16) and (17) are satisfied, the result is expected to be reasonable, particularly when the stress state in the material is effectively 2-D (such as the ruby sensor in the plate impact experiments). The accuracy for using (16) and (18) depends strongly on the ratio of the $z$-axis compression over the lateral compression. When the lateral compression diminishes, it is better to use (9) and (10) instead of (16) and (18).

## D. Models for $\alpha$-Quartz

### 1) Hugoniot equations for designing experiment:

The elastic response of $\alpha$-quartz shock-compressed along the $x$-axis was reported in Ref. 2 through the following expression:

$$U_S^e = 5.74 - 0.14u_p \text{ (mm/μs)}, \qquad \text{for } \sigma_c \le 25 \text{ kbar}; \tag{19a}$$

and

$$U_S^e = 5.57 + 1.08u_p \text{ (mm/μs)}, \qquad \text{for } 25 \text{ kbar} < \sigma_c \le 50 \text{ kbar}. \tag{19b}$$

Equation (19a) indicates that the material under $x$-axis uniaxial compression has a somewhat dispersive response instead of shocking up. However, as suggested in Ref. 2, the experimental data can be approximated using a constant wave speed of 5.728 mm/μs for an accuracy better than 0.5%. The calculated Hugoniot response using this approximation, (19b), an initial density of 2.65 g/cm$^3$, and the jump conditions is presented in Fig. 4 as the solid lines.

The shock stress-particle velocity relation for $x$-cut $\alpha$-quartz is given in Ref. 17 as

$$\sigma_c = 151.6u_p \text{ (kbar)} \qquad \text{for } \sigma_c \le 25 \text{ kbar} \tag{20a}$$

and $$\sigma_c = 148.76u_p + 23.56u_p^2 \text{ (kbar)} \quad \text{for } \sigma_c > 25 \text{ kbar.} \tag{20b}$$

The corresponding $\sigma_c - \mu$ curve is also shown in Fig. 4 as the dotted lines. The difference between the results of (19) and (20) is negligibly small. The two representations can be used as a consistent set of Hugoniot equations for designing experiment. Note, that we use $x$-cut $\alpha$-quartz primarily as stress gauge. Reasonable linearization for the piezoelectric response of quartz gauge holds only up to 40 kbar shock stress[14] even though the mechanical elastic limit may be beyond this value. For this reason, we are only interested in the shock response of the material up to 40 kbar (Fig. 4).

The HEL for $\alpha$-quartz shocked along the $z$ axis may be slightly above 60 kbar.[5] The elastic shock response of $z$-cut $\alpha$-quartz was characterized in Ref. 3 as

$$U_S^e = 6.36 + 1.36u_p \text{ (mm/μs).} \tag{21}$$

The corresponding $\sigma_c - u_p$ relation is

$$\sigma_c = 168.54u_p + 36.04u_p^2 \text{ (kbar).} \tag{22}$$

The corresponding $\sigma_c - \mu$ curve is plotted in Fig. 5 as the dotted line.

**2) Models for wave code computation:**

Again, the finite-strain elastic calculation presentd in Sec. B is used to derive the necessary equations. The material constants available are:[7-9]

$$C_{1111}^S = 868 \text{ kbar},\ C_{3333}^S = 1057.5 \text{ kbar},\ C_{1122}^S = 70.4 \text{ kbar},\ C_{1133}^S = 119.1 \text{ kbar},$$

$$C_{111111}^S = -2100 \text{ kbar},\ C_{333333}^S = -8150 \text{ kbar},$$

$$C_{111122}^S = -3450 \text{ kbar},\ C_{111133}^S = +120 \text{ kbar},\ C_{113333}^S = -3120 \text{ kbar},$$

$$C_{11111111}^S = 159300 \text{ kbar, and } C_{33333333}^S = 184900 \text{ kbar}.$$

For uniaxial compression along the $x$ or $z$ axis, these data suffice longitudinal stress calculations to fourth order but only to third order for lateral stress. A comparison of third and fourth order calculations for longitudinal stress is also shown in Fig. 5. For

each of the two compressions, the difference is significant. A further note is that the fourth order constants were actually inferred from the difference between the shock compression data and elastic calculations to third order.[9] Clearly, for our purpose (shock wave studies), we need to use the more accurate fourth order calculations for longitudinal stress. However, in the absence of necessary elastic constants for calculating mean stress to fourth order, we use the third order calculations (shown also in Fig. 5) as approximation. The computational models given in the following are only accurate for longitudinal stress but not for lateral stress even under the uniaxial-strain condition.

For *x-axis compression*, the computational model is

$$P_H = 352.5\mu + 146.6\mu^2 - 963.5\mu^3 \text{ (kbar)}, \tag{23}$$

and

$$G = 386.6 - 3.484P + 0.3121P^2 \text{ (kbar)}. \tag{24}$$

For *z-axis compression*, the model is

$$P_H = 431.9\mu + 1463\mu^2 - 4919\mu^3 \text{ (kbar)}, \tag{25}$$

and

$$G = 469.2 + 1.947P + 0.1229P^2 \text{ (kbar)}. \tag{26}$$

The $P - P_H$ relationship follows (11) and $\Gamma / V = 2 / V_0$ (an approximation using the Gruneisen parameter for fused silica[13]). In Fig. 6, the peak state results calculated using (23) to (26) are compared with the calculations using elastic constants. They are practically identical.

## D. Models for Lithium Fluoride

### 1) Hugoniot equations for designing experiment:

Given in Ref. 10, the initial density of pure LiF is 2.640 g/cm$^3$, and the shock response of the material in ⟨100⟩ orientation is

$$U_S = 5.148 + 1.353u_p \text{ (mm/μs)}, \tag{27}$$

where $U_S$ is the shock speed. Because the HEL value for ⟨100⟩ compression is negligibly small, the jump conditions directly provide the $\sigma_c - u_p$ relation,

$$\sigma_c = 135.9u_p + 35.72u_p^2 \text{ (kbar)}. \tag{28}$$

The corresponding $\sigma_c - \mu$ curve is shown in Fig. 7 as the solid line. The existing data for the Hugoniot response and optical property calibration of pure LiF subjected to shock compression in [100] direction are up to more than 1000 kbar.[10,11] However, only the Hugoniot response below 300 kbar is presented here. This range of shock stress allows us to accurately fit the material response with a cubic function and should also suffice our experimental needs.

**2) Model for wave code computation:**

Under the uniaxial-strain condition, the material response can be modeled as that of a fluid. A cubic function that fits the $\sigma_c - \mu$ curve (the solid line in Fig. 7) is used as the Hugoniot mean stress, *i.e.*,

$$P_H = 699.7\mu + 1174\mu^2 + 942.1\mu^3 \text{ (kbar)}. \tag{29}$$

The thermodynamic mean stress follows (11) and $\Gamma / V = 1.63 / V_0$.[10] Setting the equivalent shear modulus,

$$G = 0 \tag{30}$$

enables the computed peak state stress to recover the Hugoniot response given in Ref. 10 as shown in Fig. 7.

**E. Models for fused silica**

**1) Equations for designing experiment:**

Experimental measurements of the longitudinal response of fused silica subjected to uniaxial-strain stress-wave compression were reported in Ref. 1 up to a peak stress of 66 kbar. The response is non-linear elastic, displaying ramp wave at low stresses and shock beyond 40 kbar. The initial density of the material is 2.201 g/cm$^3$. The compressive longitudinal stress-particle velocity relation from Ref. 1 is

$$\sigma_c = 131.7u_p - 73.61u_p^2 + 99.47u_p^3 - 41.63u_p^4 \text{ (kbar)}. \tag{31}$$

The corresponding $\sigma_c - \mu$ relation is

$$\sigma_c = 776.0\frac{\mu}{1+\mu} - 4159\frac{\mu^2}{(1+\mu)^2} + 30340\frac{\mu^3}{(1+\mu)^3} - 69260\frac{\mu^4}{(1+\mu)^4} \text{ (kbar). (32)}$$

Note, that the longitudinal sound speed of the material under the ambient conditions was measured to be $5.93 \pm 0.01$ mm/μs.[1] However, the values inferred from (31) and (32) are 5.984 and 5.938 mm/μs, respectively. For consistency, we recommend to use the value of 5.938 mm/μs. A plot of (32) is given in Fig. 8 as the solid line.

**2) Model for wave code computation:**

The necessary information for a complete characterization of the non-linear elastic response of fused silica under uniaxial-strain, stress wave compression was obtained from the combined compression and shear wave measurements in the material.[12] It was found that the shear wave velocity, $c_S$ changes with $\mu$ in the following way:

$$c_S = 3.73 - 9.35\mu \text{ (mm/μs)} \qquad \text{for } \mu \le 0.076 \qquad \text{(33a)}$$

and

$$c_S = 2.80 + 2.90\mu \text{ (mm/μs)} \qquad \text{for } 0.076 < \mu < 0.12. \qquad \text{(33b)}$$

Using (32) and (33), and treating the uniaxially compressed material as an isotropic solid, we can calculate the bulk modulus and further integrate it over the volume compression to obtain the mean stress response of the compressed material. The result is also shown in Fig. 8. Fitting the result as a fourth order polynomial, we obtain the Hugoniot mean stress response as

$$P_H = 367.7\mu - 3907\mu^2 + 37510\mu^3 - 130100\mu^4 \text{ (kbar).} \qquad \text{(34)}$$

The shear modulus is expressed using two linear functions of $\mu$ that best fit (33):

$$G = 306.2 - 1199\mu \text{ (kbar)} \qquad \text{for } \mu \le 0.076 \qquad \text{(35a)}$$

and

$$G = 215.076 + 668.4(\mu - 0.076) \text{ (kbar)} \qquad \text{for } 0.076 < \mu < 0.12. \qquad \text{(35b)}$$

The Gruneisen parameter is $\Gamma / V = 2.0 / V_0$.[13] A comparison between (33) and (35) is presented in Fig. 9. The computed peak state response matches the experimental results to 60 kbar very well as shown in Fig. 8. Direct extension to higher stresses is not recommended because the slope of (34) may be negative. See one of us (RF) for further details of using this model in the COPS code. Note, that the mean stress analysis used here (the thin dashed line in Fig. 8) yields a slightly different result than that of an earlier analysis reported in Ref. 18, where two numerical constants were rounded slightly during the derivation. The best fourth order fit to that result is

$$P_H = 367.7\mu - 3738\mu^2 + 35210\mu^3 - 120500\mu^4 \text{ (kbar)}. \qquad (36)$$

This has so far been used in all of the COPS and TROTT code calculations involving fused silica. As shown in Fig. 8, the peak state results calculated using (35) and (36) are slightly stiffer than experimental results. The largest difference is about 0.5 kbar, which should be well within the experimental error. For consistency, however, we recommend to use (34) and (35) from now on.

**References:**

[1]L. M. Barker and R. E. Hollenbach, J. Appl. Phys. **41**, 4208 (1970).

[2]R. A. Graham, F. W. Neilson, and W. B. Benedick, J. Appl. Phys. **36**, 1775 (1965).

[3]J. Wackerle, J. Appl. Phys. **33**, 922 (1962).

[4]P. D. Horn and Y. M. Gupta, Phys. Rev. B **39**, 973 (1989).

[5]S. M. Gallivan, M.S. Thesis, Washington State University, Pullman, WA, 1993.

[6]R. E. Hankey and D. E. Schuele, J. Acoust. Soc. Am. **48**, 190 (1970).

[7]H. J. McSkimin, P. Andreatch, Jr., and R. N. Thurston, J. Appl. Phys. **36**, 1624 (1965).

[8]R. N. Thurston, H. J. McSkimin, and P. Andreatch, Jr., J. Appl. Phys. **37**, 267 (1966).

[9]R. Fowles, J. Geophys. Res. **72**, 5729 (1967).

[10]W. J. Carter, High Temp.-High Press. **5**, 313 (1973).

[11]J. L. Wise and L. C. Chhabildas, in Shock Waves in Condensed Matter, edited by Y. M. Gupta (Plenum Press, New York, 1986), p. 441.

[12]M. P. Conner, M.S. Thesis, Washington State University, Pullman, WA, 1988.

[13]R. L. Gustavsen, Ph.D. Thesis, Washington State University, Pullman, WA, 1989.

[14]H. d'Amour, D. Schifel, W. Denner, Heinz Schulz, and W. B. Holzapfel, J. Appl. Phys. **49**, 4411 (1978).

[15]F. D. Murnaghan, *Finite Deformation of an Elastic Solid* (Dover, New York, 1967).

[16]W. A. Bassett, M. S. Weathers, T.-C. Wu, and T. Holmquist, J. Appl. Phys. **74**, 3824 (1993).

[17]Z. P. Tang, Y. M. Gupta, and P. M. Bellamy, Rev. Sci. Instrum. **59**, 1189 (1988).

[18]M. K. W. Wong, Ph.D. Thesis, Washington State University, Pullman, WA, 1991.

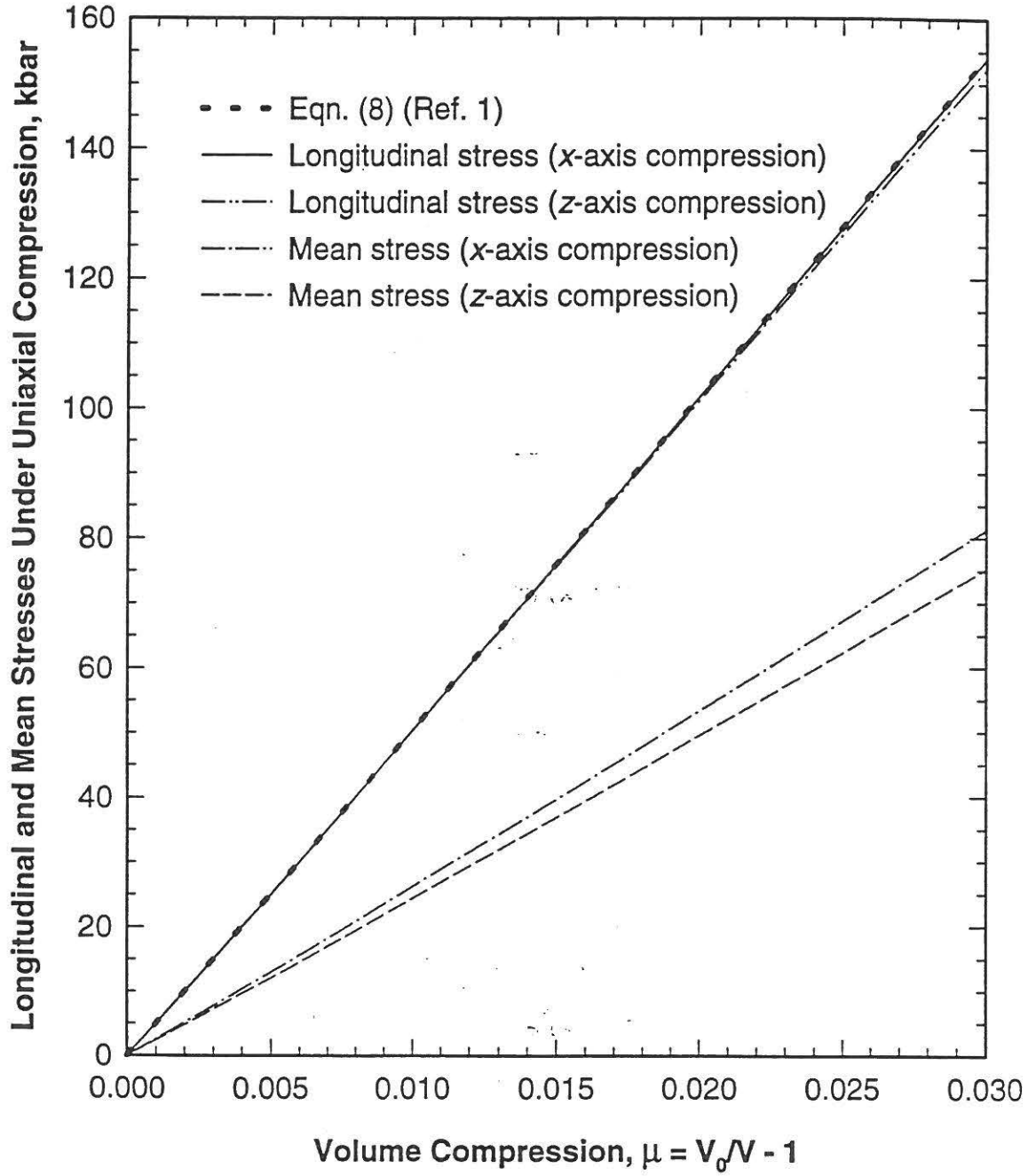


Fig. 1, Material response of sapphire under uniaxial-strain $z$-axis or $x$-axis compression: the measured shock response of $z$-cut sapphire (Ref. 1), and the calculated longitudinal and mean stresses using third order elastic constants (Ref. 6) for the two compressions.

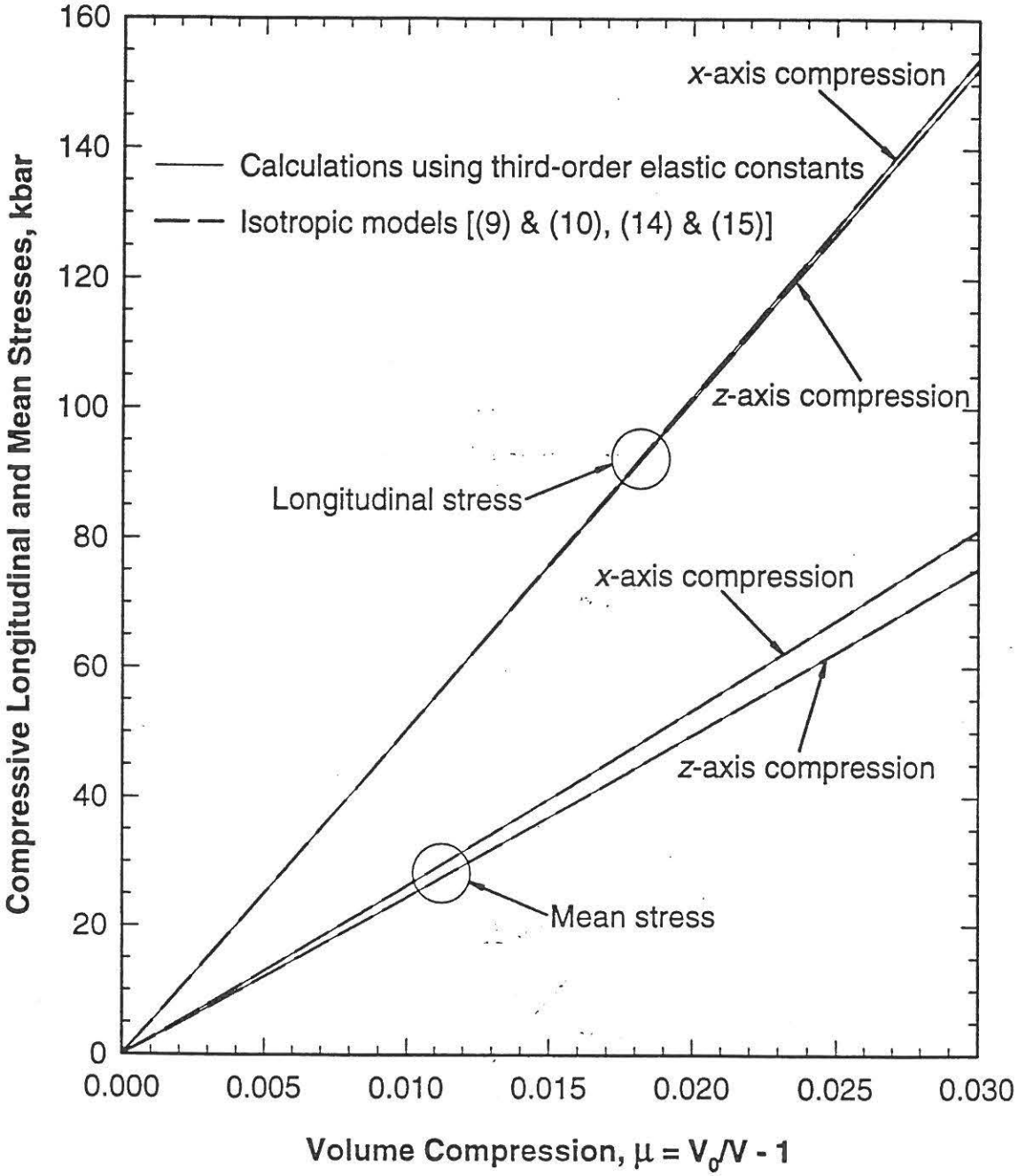


Fig. 2, Comparison of calculations using third order elastic constants and peak state results of 1-D isotropic models for sapphire response under uniaxial-strain, $x$-axis or $z$-axis compression.

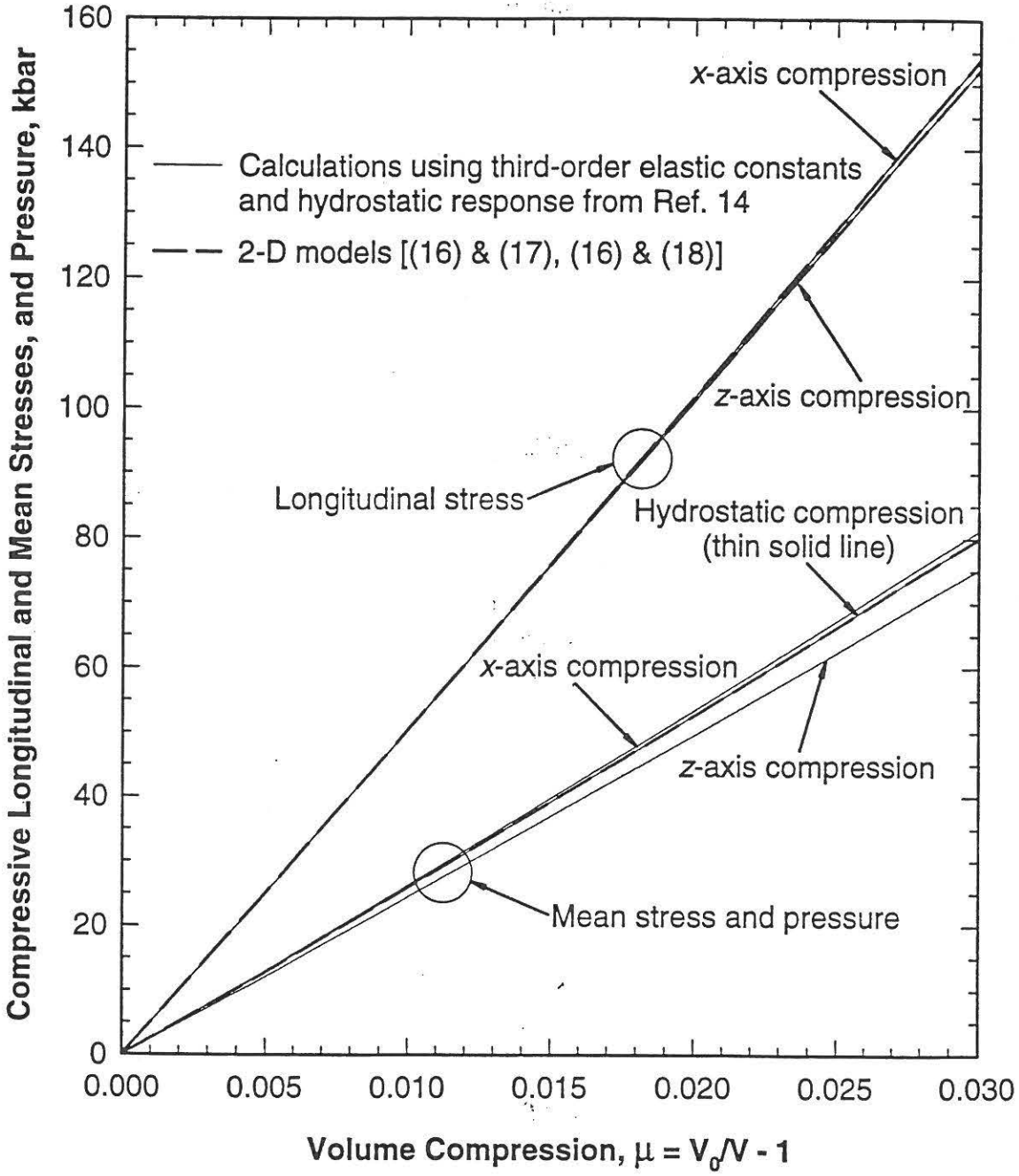


Fig. 3, Comparison of material response of sapphire under uniaxial-strain and hydrostatic compressions, and peak state results of 2-D models.

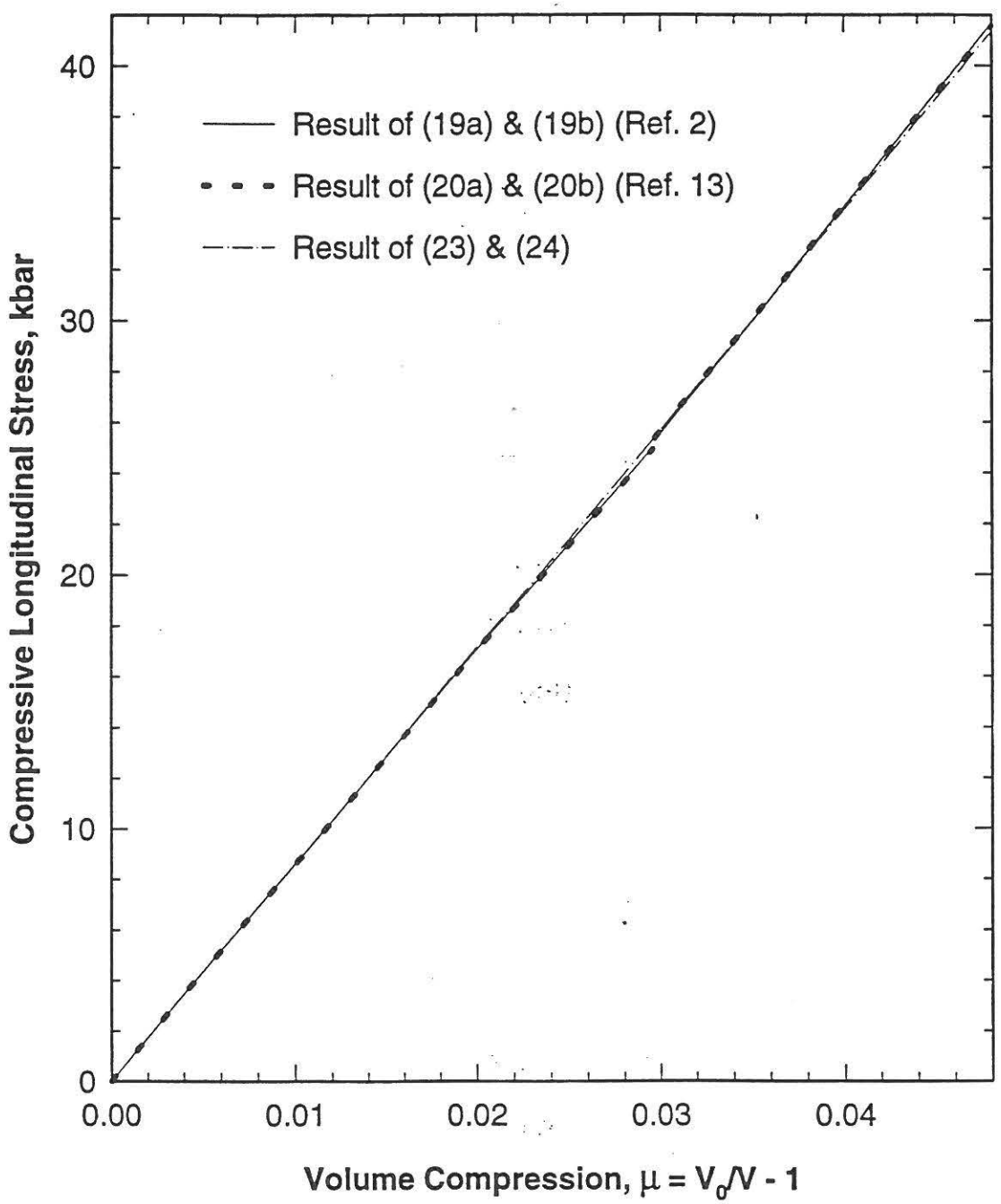


Fig. 4, Material response of $\alpha$-quartz under uniaxial-strain $x$-axis compression: the measured shock response of $x$-cut quartz (Ref. 2), the result of shock stress-particle velocity model for $x$-cut quartz (Ref. 13), and the result of computational model derived from calculations using higher order elastic constants (Refs. 7-9).

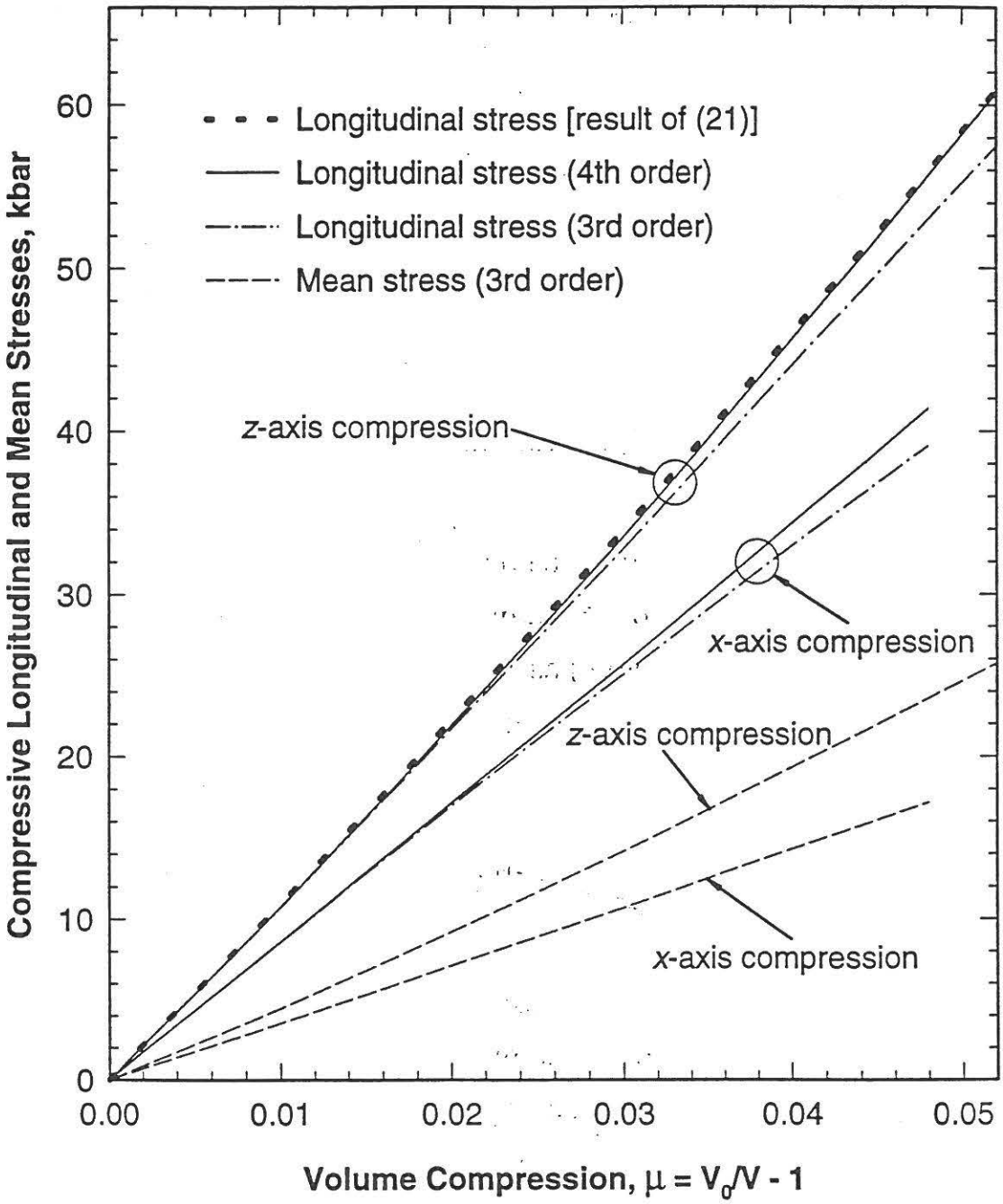


Fig. 5, Elastic response of $\alpha$-quartz under uniaxial-strain $z$-axis or $x$-axis compression: the measured shock response of z-cut quartz (Ref. 3), and the calculated longitudinal stresses (using elastic constants to third or fourth order, Refs. 7-9) and mean stress (to third order) for the two compressions.

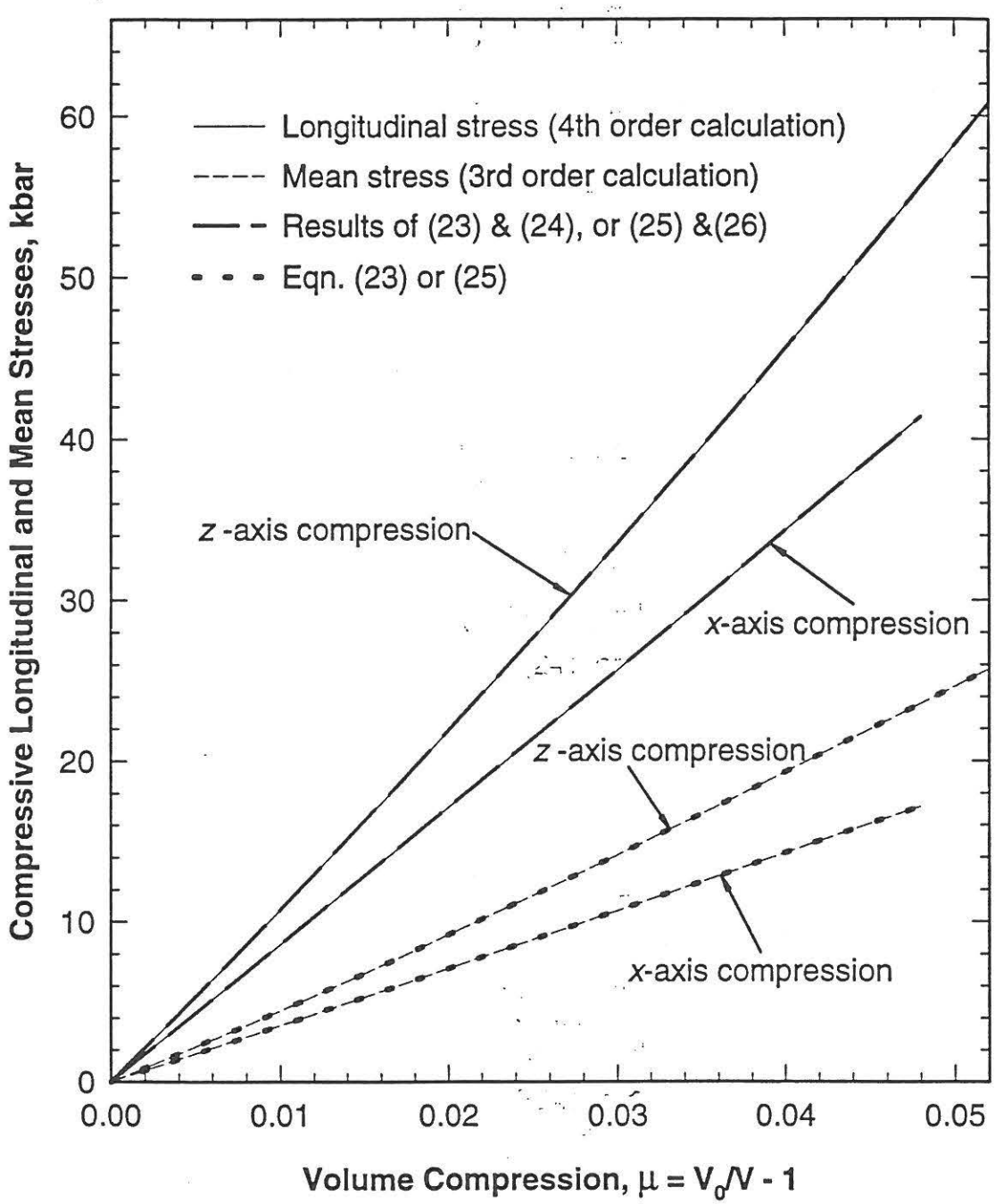


Fig. 6, Comparison of calculations using higher order elastic constants and peak state results of computational models for $\alpha$-quartz response under uniaxial-strain $x$-axis or $z$-axis compression.

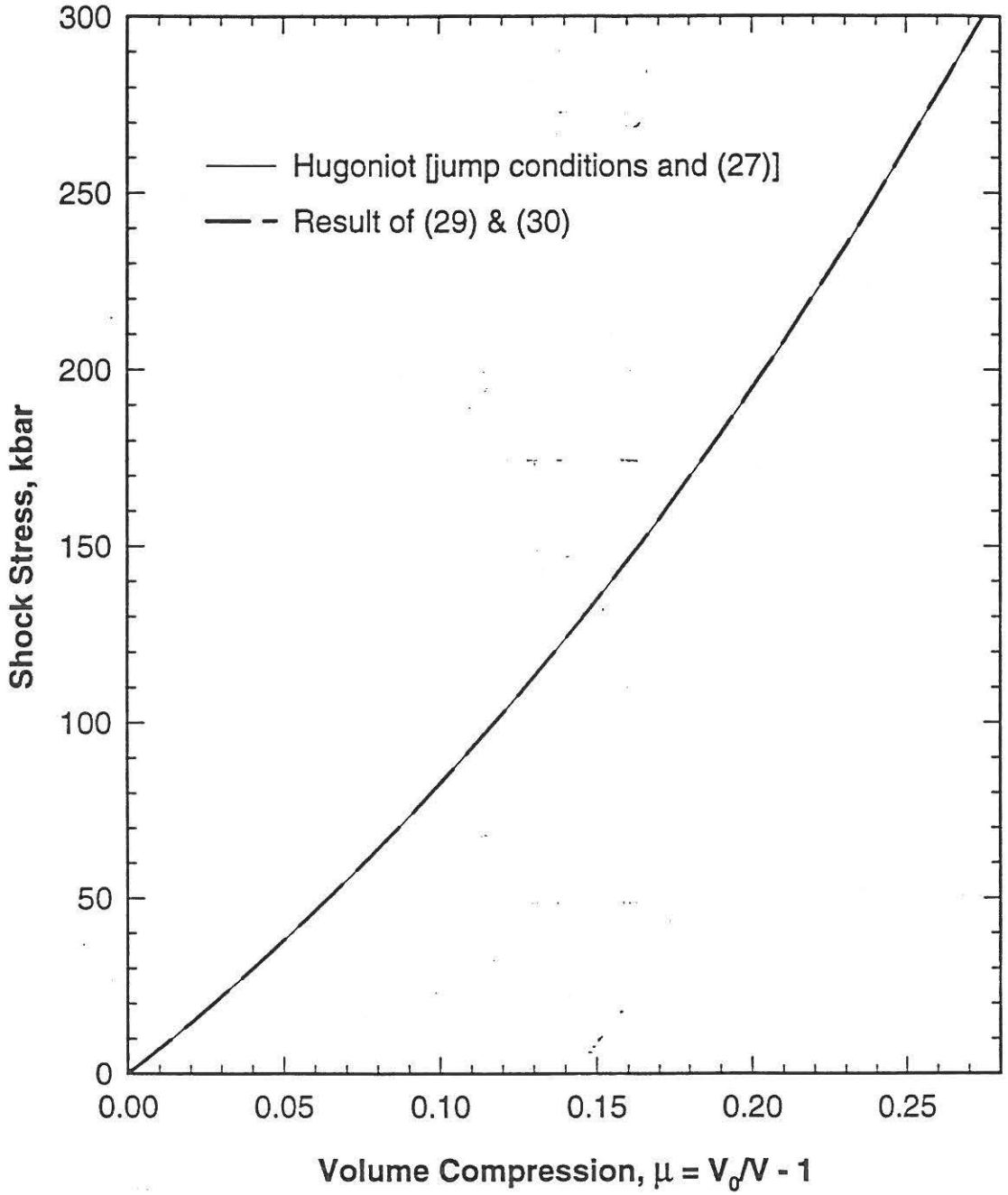


Fig. 7, Shock response of pure lithium fluoride in ⟨100⟩ orientation (up to 300 kbar): The Hugoniot response given in Ref. 10 is compared with the peak state result of computational model.

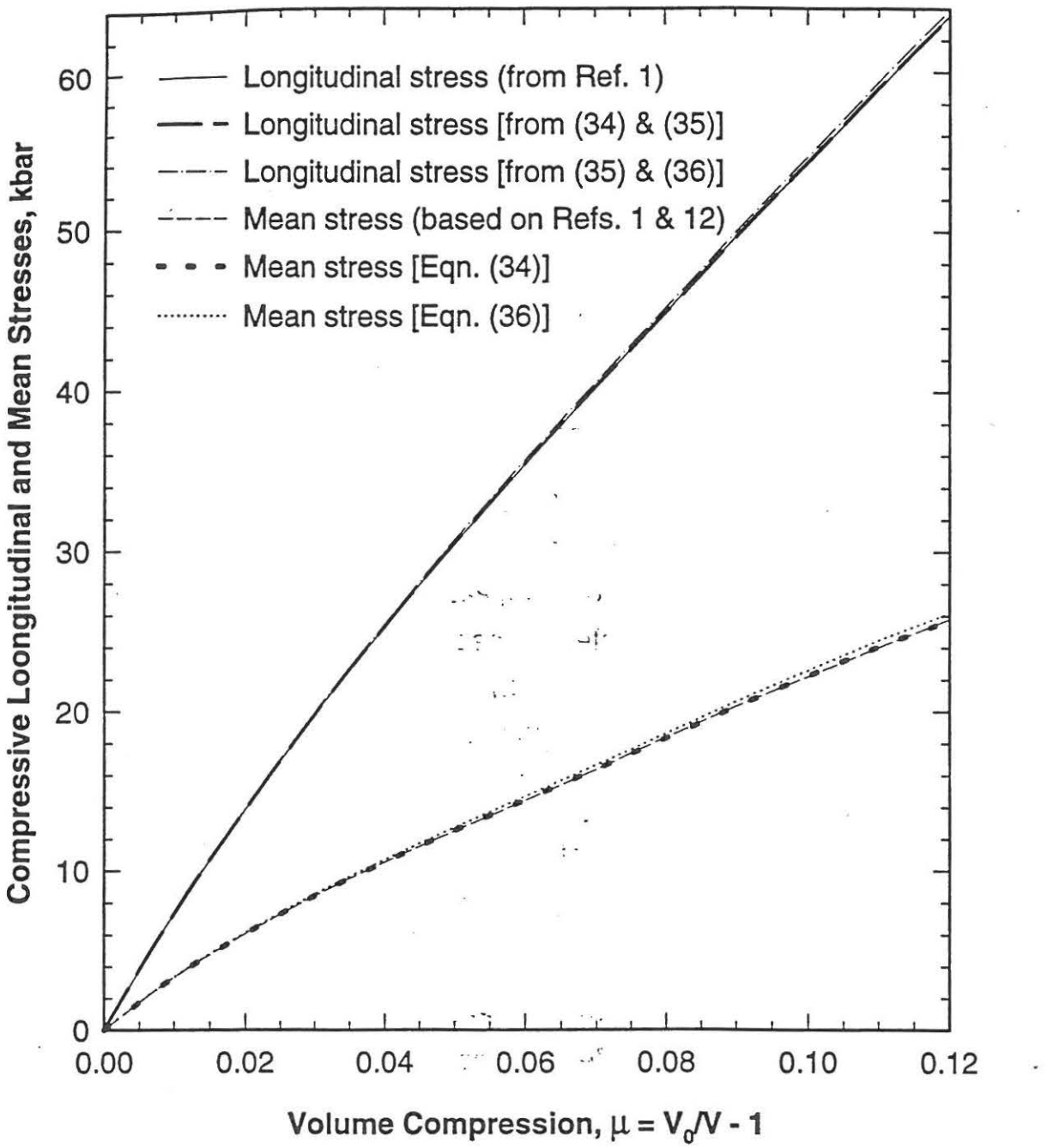


Fig. 8, Material response of fused silica under uniaxial-strain, shock wave compression: the experimental results on the longitudinal and mean stresses in the shocked state (Refs. 1 & 12), the peak state results of the computational model from this work, and the peak state results of the model previously used in the COPS and TROTT codes.

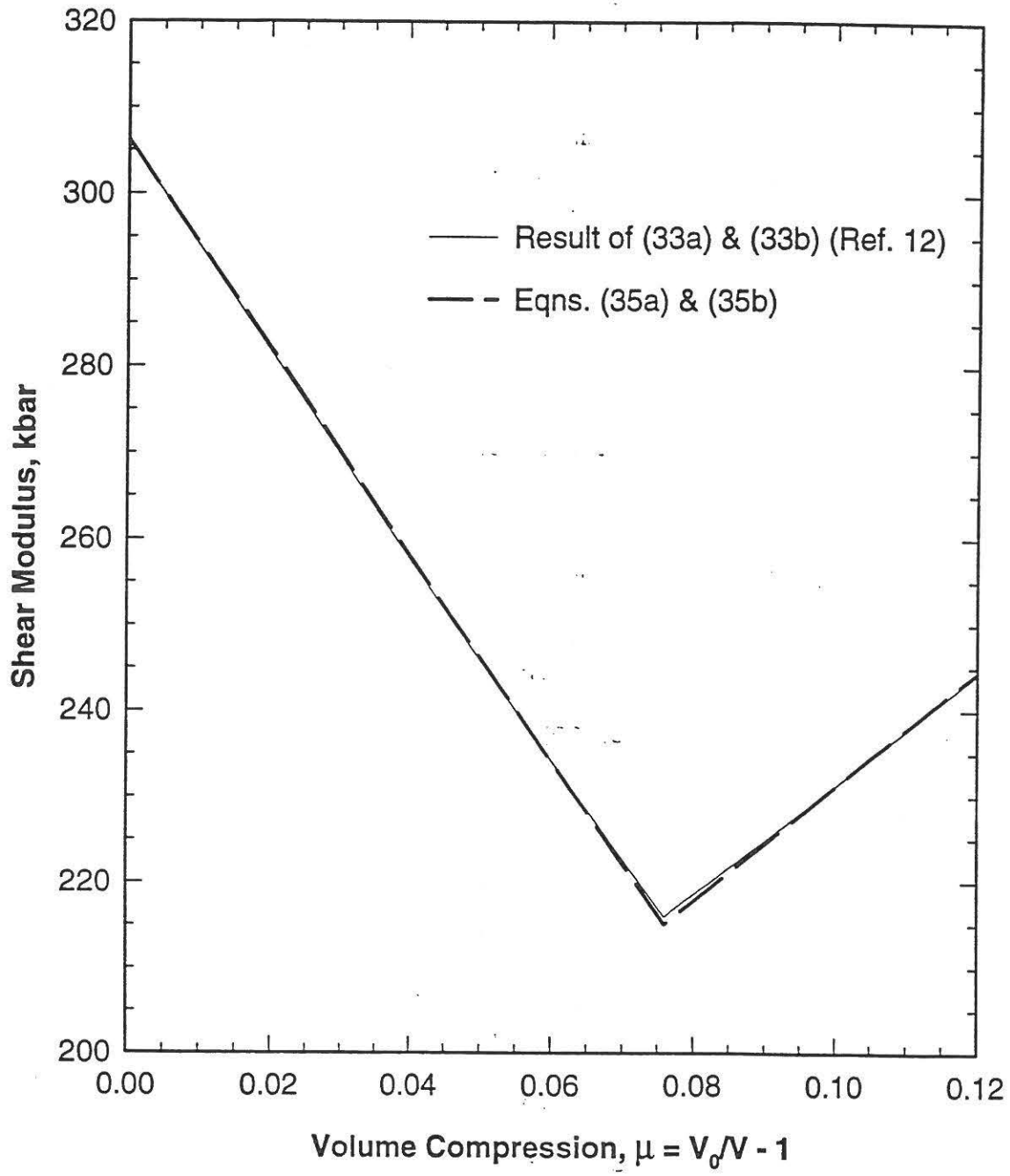


Fig. 9, Shear modulus of fused silica in the shocked state: The computational model is compared with the experimental result from Ref. 12.